Telomere shortening produces an inflammatory environment that increases tumor incidence in zebrafish

Kirsten Lex[a,1], Mariana Maia Gil[a,1], Bruno Lopes-Bastos[a,b], Margarida Figueira[a], Marta Marzullo[a], Kety Giannetti[a], Tânia Carvalho[c], and Miguel Godinho Ferreira[a,b,2]

[a]Telomere and Genome Stability Laboratory, Instituto Gulbenkian de Ciência, 2781-901 Oeiras, Portugal; [b]Institute for Research on Cancer and Aging of Nice (IRCAN), Université Côte d'Azur, UMR7284 U1081 UNS, 06107 Nice, France; and [c]Champalimaud Centre for the Unknown, Champalimaud Foundation, Av Brasilia, 1400-038 Lisbon, Portugal

Edited by Ronald A. DePinho, University of Texas MD Anderson Cancer Center, Houston, TX, and approved May 18, 2020 (received for review November 15, 2019)

Cancer incidence increases exponentially with age when human telomeres are shorter. Similarly, telomerase reverse transcriptase (*tert*) mutant zebrafish have premature short telomeres and anticipate cancer incidence to younger ages. However, because short telomeres constitute a road block to cell proliferation, telomere shortening is currently viewed as a tumor suppressor mechanism and should protect from cancer. This conundrum is not fully understood. In our current study, we report that telomere shortening promotes cancer in a noncell autonomous manner. Using zebrafish chimeras, we show increased incidence of invasive melanoma when wild-type (WT) tumors are generated in *tert* mutant zebrafish. Tissues adjacent to melanoma lesions (skin) and distant organs (intestine) in *tert* mutants exhibited higher levels of senescence and inflammation. In addition, we transferred second generation (G2) *tert* blastula cells into WT to produce embryo chimeras. Cells with very short telomeres induced increased tumor necrosis factor1-α (TNF1-α) expression and senescence in larval tissues in a noncell autonomous manner, creating an inflammatory environment. Considering that inflammation is protumorigenic, we transplanted melanoma-derived cells into G2 *tert* zebrafish embryos and observed that tissue environment with short telomeres leads to increased tumor development. To test if inflammation was necessary for this effect, we treated melanoma transplants with nonsteroid anti-inflammatory drugs and show that higher melanoma dissemination can be averted. Thus, apart from the cell autonomous role of short telomeres in contributing to genome instability, we propose that telomere shortening with age causes systemic chronic inflammation leading to increased tumor incidence.

telomeres | telomerase | cancer | inflammation | aging

Cancer incidence increases exponentially in the mid-decades of human life (1). Although mutations are required to build up during tumorigenesis, the overall postreproductive incidence opens the possibility of organism-based causes for the increase in cancer with age. Due to the absence of telomerase expression in most somatic tissues, telomeres shorten as we grow older (2). Telomeres constitute the ends of eukaryotic chromosomes and are constituted by repetitive DNA sequences $(TTAGGG)_n$ recognized by a protein complex called shelterin (3). This structure prevents chromosome ends from being recognized as deleterious DNA double strand breaks while counteracting their slow attrition, resulting from the "end-replication problem" by recruiting telomerase. Humans are born with telomeres between 10- and 15-kb long (4) and, due to continuous cell divisions, telomeres may reach a critical length. As cell division reaches the Hayflick limit, telomeres are recognized as DNA damage and block cell proliferation either by undergoing senescence or by apoptosis (5–7).

Since short telomeres block cell division, telomere shortening is considered as a tumor suppressor mechanism by preventing excessive cell proliferation. However, short and dysfunctional telomeres cause genome instability and, thus, facilitate carcinogenesis. Previous studies suggest that telomere dysfunction triggers higher tumor initiation (8, 9), yet subsequent tumor progression appears to be limited, at least, partially, in the absence of telomerase (10, 11) and only fully active if telomerase is restored (12, 13). This idea is further supported by experiments in cancer-prone telomerase-deficient mice. Correlating with telomere shortening across the several generations of telomerase-deficient mice, the authors observe increased tumor initiation but less growth and progression into advanced tumor stages (14). Indeed, telomerase is frequently reactivated in the majority of cancer cells, allowing for cell immortalization thereby escaping replicative senescence. In line with this idea, anti-telomerase therapies are currently undergoing clinical trials for cancer therapy (15).

Countering the tumor suppressor hypothesis, telomere shortening may lead to genome instability, a hallmark of cancer. Because loss of telomere protection results in breakage-fusion-bridge cycles, the ensuing genome instability may contribute for age-dependent tumorigenesis (16). An extreme example of the protumorigenic

Significance

Cancer incidence increases exponentially in human midlife. Even though mutation accumulation in somatic tissues results in increased tumorigenesis, it is currently not understood how aging contributes to cancer. Telomeres, the ends of eukaryotic linear chromosomes, shorten with each cell division. Here, we show that telomere shortening contributes to cancer in a noncell autonomous manner. Using embryo chimeras of telomerase-deficient zebrafish generated from melanoma-prone fish, we show that tumors arise more frequently, multiply faster, and become more invasive in animals with shorter telomeres. Telomere shortening gives rise to increased senescence and systemic inflammation. We observed increased melanoma dissemination in zebrafish larvae with very short telomeres. Thus, telomere shortening similar to human aging, generates a chronic inflammatory environment that increases cancer incidence.

Author contributions: K.L., M.M.G., B.L.-B., M.F., and M.G.F. designed research; K.L., M.M.G., B.L.-B., M.F., M.M., K.G., and M.G.F. performed research; K.L., M.M.G., and M.F. contributed new reagents/analytic tools; K.L., M.M.G., B.L.-B., M.F., M.M., K.G., T.C., and M.G.F. analyzed data; M.G.F. acquired funding and coordinated the work; and K.L., M.M.G., B.L.-B., and M.G.F. wrote the paper.

The authors declare no competing interest.

This article is a PNAS Direct Submission.

[1]K.L. and M.M.G. contributed equally to this work.

[2]To whom correspondence may be addressed. Email: Miguel-Godinho.FERREIRA@unice.fr.

This article contains supporting information online at https://www.pnas.org/lookup/suppl/doi:10.1073/pnas.1920049117/-/DCSupplemental.

First published June 17, 2020.

effect of short telomeres occurs in "telomeropathies." People carrying mutations in telomerase or related proteins have pathologically short telomeres in early life (17, 18). Despite exhibiting pathologies related to deficiencies in cell proliferation, patients also suffer from an increased cancer risk (19). Similarly, our work on the telomerase mutant zebrafish, which undergoes premature telomere shortening, revealed that they anticipate cancer incidence to early life (20). Even though short telomeres positively correlate with increased tumorigenesis in both humans and zebrafish, it is not yet understood how telomere shortening may lead to cancer.

Telomere shortening has consequences beyond the cellular level. As cells approach replicative senescence, DNA damage emanating by short telomeres initiates a cascade of events that expands to the extracellular environment. Senescent cells were shown to release a set of molecules termed senescence-associated secretory phenotype (SASP) (21). SASP is described in vitro and is mainly constituted by chemokines, growth factors, extracellular matrix remodelers, and other inflammatory factors, capable of modulating cell environment. These molecules were posteriorly shown to influence the ability of other cells to divide, potentially having a protumorigenic effect (22). Consistently, repeated wounding in zebrafish stimulates inflammatory responses, which were shown to promote cancer progression (23, 24). Therefore, we hypothesize that telomere shortening contribution to tumorigenesis may have a noncell autonomous component. In aging organisms, cells undergoing replicative senescence would comprise a source of SASP/inflammatory factors creating a protumorigenic environment. In agreement with our hypothesis, population studies have associated the long-term use of anti-inflammatory agents (acetylsalicylic acid) and a reduction risk of several cancers (25–27).

Here, we show that tissues containing cells with short telomeres promote increased cancer incidence in a noncell autonomous manner. Using chimeric zebrafish, we observed that telomerase-proficient melanocytes expressing HRAS give rise to more melanoma tumors when surrounded by *tert* mutant cells. Melanomas developed in this environment exhibited high invasiveness as observed by histopathology. In agreement, using zebrafish tumor transplants, we show that HRAS melanoma cells expand faster when injected into G2 *tert* mutant larvae. Both adult first generation (G1) *tert* and G2 *tert* larvae have higher levels of senescence and SASP/inflammation. G2 *tert* cells injected into WT embryos stimulate senescence and inflammation in a noncell autonomous manner. Chemical inhibition of inflammation in G2 *tert* embryos rescued the higher dissemination of melanoma cells. Thus, cells with short telomeres are capable of inducing senescence and inflammation, creating a protumorigenic environment that results in higher cancer incidence.

Results

***tert* Mutant Environment Causes Higher Tumor Incidence in a Noncell Autonomous Manner.** Similar to mammals, zebrafish tumor microenvironment (TME) modulates cancer behavior (28, 29). Tumors may be inhibited or enhanced as a consequence of the dynamic cross talk between cancer and surrounding cells. We, therefore, asked what were the effects of a TME with short telomeres on emergent tumors.

In order to study the noncell autonomous effects of TME telomere shortening in cancer, we wanted to separate telomerase expression of precancer cells from their surrounding tissues and, for this purpose, we generated chimeric zebrafish using early-developmental embryo transplants. We used a melanoma zebrafish model (*mitfa*:HRAS) developed by the Hurlstone Laboratory that exhibits full penetrance by 3 months of age (30). We chose this model since it does not carry a *tp53* germline mutation. Other melanoma models, such as the *mitfa:BRAF^{V600E}* zebrafish line, are dependent on *tp53* germline dysfunction to form tumors (31), and we had previously shown that loss of the p53 function suppresses *tert* zebrafish phenotypes (32). Blastula cells from donor embryos capable of giving rise to melanoma were transplanted into WT or *tert$^{hu3430/hu3430}$* homozygous mutants (*tert$^{-/-}$*) recipients (Fig. 1*A*). In addition, recipient embryos had a *casper* genetic background (*mitfa$^{w2/w2}$; mpv17$^{a9/a9}$*) and lacked the ability to produce melanocytes. Consequently, all melanomas could only arise from donor cells. Embryo chimeras then were allowed to grow into adulthood and studied for tumor incidence. As expected, we observed the development of melanoma lesions, typically in the anal fin region of both WT and *tert$^{-/-}$* recipient fish (Fig. 1*B*). However, by 30 weeks, a time when *tert$^{-/-}$*-associated lethality is still low (<20%), 20% of WT chimeras developed tumors, while ca. 50% of *tert$^{-/-}$* chimeras exhibited melanoma (Fig. 1*C*, $P < 0.05$). Thus, we found that *tert$^{-/-}$* recipients significantly increased tumor incidence by ca. twofold (Hazard ratio after Mantel–Haenszel calculation: 2.0 when compared with WT fish).

A possible explanation for the observed differences of tumor development in a WT vs. *tert$^{-/-}$* environment is cell competition. WT tumor-prone cells could be fitter and more efficient in outcompeting *tert* mutant recipient cells, possibly due to higher proliferation rates. Thus, fitter donor cells could produce a higher number of melanocytes expressing HRAS in *tert* mutant recipients and, subsequently, lead to a higher tumor incidence. To test this hypothesis, we quantified the number of melanocytes at two stages of embryo development at 3- and 11-d post-fertilization (dpf) in both *tert* mutant and WT recipients. Contrary to our hypothesis, we observed no significant increase in the number of melanocytes in *tert$^{-/-}$* recipients as compared to WT during developmental stages (*SI Appendix*, Fig. S1 *A–E*). In case growth differences would only be visible at later stages, we quantified the surface area covered by the melanocytic lesions in adult animals. Percentage of pigmentation was quantified for WT and *tert$^{-/-}$* zebrafish (*SI Appendix*, Fig. S1 *F* and *G*). Similar to the results obtained in larvae, although there was variation between individuals, we did not observe significant differences when comparing host genotypes. Together, our data indicate that a *tert* mutant TME increases tumor incidence in a noncell autonomous manner, suggesting that telomere shortening plays a

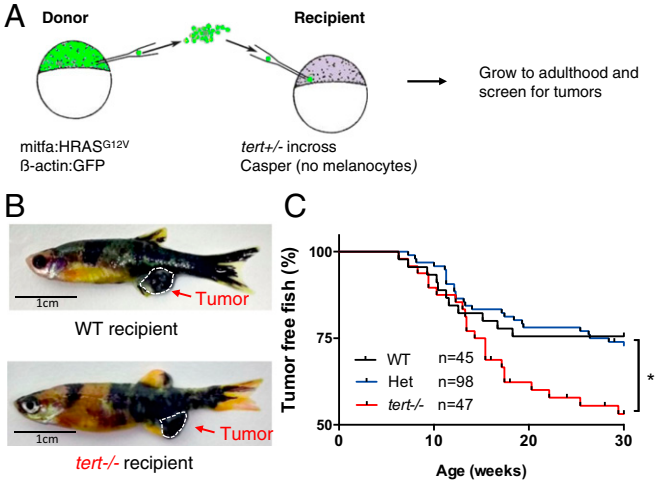

Fig. 1. Short telomeres promote tumorigenesis in a noncell autonomous manner. (*A*) Experimental setup for the generation of zebrafish chimeras. Donor cells are transplanted from a Tg(*mitfa:HRAS^{G12V}; β-actin:GFP*) embryo at the blastula stage into embryos resulting from an in cross of *tert$^{+/-}$*; casper zebrafish. (*B*) Representative images of adult chimera zebrafish harboring melanoma in either WT or *tert$^{-/-}$* recipients. (*C*) Melanoma occurrence over time in chimeric fish. *tert$^{-/-}$* recipient fish have a higher risk of tumorigenesis than WT and het recipient fish. *$P < 0.05$.

systemic role in cancer beyond the one described in genome stability.

Tumors Progress Faster in *tert* Mutant TME. Among the hallmarks of cancer, one qualitative difference between cancers relies on the capacity to invade different tissues. Zebrafish chimeras bearing melanoma were analyzed by histopathology and ranked according to their staging and invasiveness. Overall, 84% of samples (n = 43) that were macroscopically defined as tumors were confirmed as malignant tumors in histopathological analysis (Fig. 2 *A* and *B*). The remaining samples were staged as benign tumors or melanosis. The large majority of tumors in $tert^{-/-}$ recipients were invasive (80%, n = 10; Fig. 2*B*). In comparison, only 22% of tumors exposed to a WT environment (n = 9) were determined as invasive (Fig. 2*B*). A similar result was found when malignant tumors were scored for the presence of cellular atypia. Cellular atypia describes cytologic structural abnormalities and is a marker for more transformed cancers and more advanced staging (33). Whereas 71% of tumors in a $tert^{-/-}$ environment (n = 7) exhibited moderate levels of cellular atypia (Fig. 2*C*), all tumors in WT recipients showed low levels (n = 5). In addition, we observed that melanoma cells in the $tert^{-/-}$ TME increase their proliferation capacity in comparison to WT (93.7% vs. 80%, $P < 0.01$; $n = 3$) as indicated by proliferating cell nuclear antigen (PCNA) staining (Fig. 2 D and *E*). These results indicate that melanoma developed in $tert^{-/-}$ recipients develop faster, reaching advanced stages faster and becoming more invasive, suggesting that TME telomere shortening not only increases tumor incidence, but also increases its progression.

Zebrafish Melanoma Transplants Disseminate Faster in *tert* Mutant Larvae. We and others have shown that injection of tumor cells in zebrafish larvae constitutes an assay to study invasiveness capacity of cancer cells (34, 35). This constitutes a simpler assay and allows for more expedite manipulations while being amenable to chemical studies.

In order to confirm that $tert^{-/-}$ TME promotes tumor dissemination, we injected melanoma cells derived from HRAS tumors into 2-dpf WT and $tert^{-/-}$ larvae (Fig. 3*A*). To ensure that these fish would possess cells with critically short telomeres, we

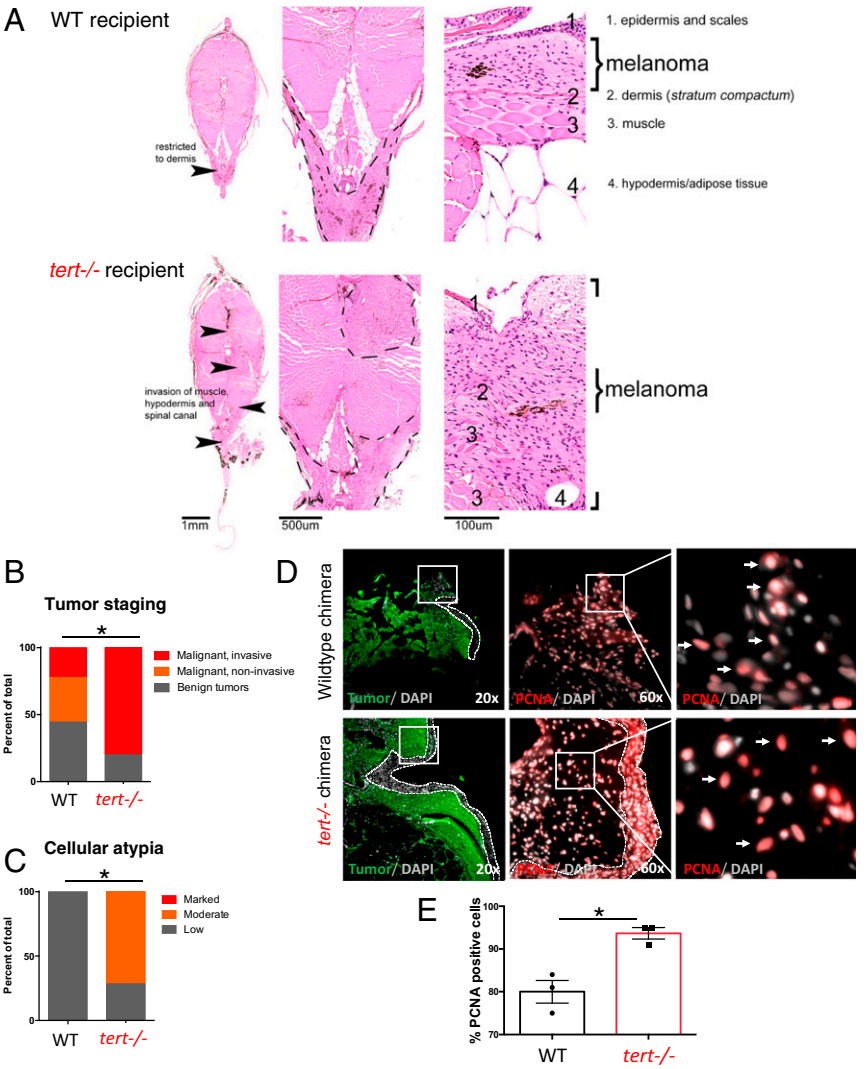

Fig. 2. $tert^{-/-}$ tissues increase melanoma invasiveness and progression. (*A*) Hematoxylin and eosin (H and E) images of melanoma arising in a WT (*Upper*) or $tert^{-/-}$ recipient fish. Strong infiltration into other tissues was typical in $tert^{-/-}$ fish but not in WT (arrowheads). (*B*) Melanomas were staged according to histopathology into benign lesions (melanosis), noninvasive and invasive malignant tumors (P = 0.0269; WT n = 9; $tert^{-/-}$ n = 10). (*C*) Analysis of malignant tumors for cellular atypia (P = 0.0278; WT n = 5; $tert^{-/-}$ n = 7). (*D*) Representative immunofluorescence images of PCNA-positive cells (red) in melanoma (green) developed in WT chimeras and in $tert^{-/-}$ chimeras. Dashed lines locate the skin (no green fluorescence), squares show the place of amplification, and arrows indicate PCNA-positive cells. (*E*) Quantification of PCNA-positive melanoma cells in WT and $tert^{-/-}$ chimeras. Data are represented as mean ± SEM. *$P < 0.05$; n = 3.

used G2 *tert*$^{-/-}$ resulting from an in cross of young adult *tert*$^{-/-}$ zebrafish. In contrast to G1 *tert*$^{-/-}$ derived from heterozygous parents, G2 *tert*$^{-/-}$ embryos possess very short telomeres and a high mortality with an average longevity of ~12 days (32, 36). We dissected melanomas from HRAS tumors expressing green fluorescent protein (GFP) (see *Methods*) and injected cells into the blood circulation of 2 days postfertilization (dpf) larvae. Injected melanoma cells preferentially accumulate in the tail region from where, depending on their invasiveness capacity, they disseminate to neighboring tissues (Fig. 3*B*). Injected larvae were individually followed over time, and the area occupied by GFP cells was quantified (Fig. 3*B*).

If an environment with short telomeres promotes tumor growth and expansion, then injected melanoma cells should disseminate more when injected in G2 *tert*$^{-/-}$ when compared to WT larvae. We quantified the GFP area at 1-, 4-, and 7 days postinjection (dpi) (Fig. 3*C*). We calculated the linear regression among the three time points and obtained a progression slope for the expansion of each grafted melanoma (Fig. 3*D*). Rather than comparing individual time points, we resorted to using the progression slope since it better represented the rate of increase in the tumor area over time and would be independent of the exact number of cells injected. We observed that *tert*$^{-/-}$ recipients allowed for a more accentuated progression than the WT ones (Fig. 3*D*, WT $n = 32$; *tert*$^{-/-}$ $n = 31$; $P = 0.0205$). As we observed increased tumor invasiveness as well as increased cell proliferation of melanoma cells in adult *tert*$^{-/-}$ chimeras (Fig. 2), we anticipated both tumor dissemination and cell proliferation may contribute to the observed results. However, further studies will explore the independent contribution of these properties on the increased tumor incidence of *tert*$^{-/-}$ chimeras. Overall, our results using tumor transplants indicate that melanoma cells disseminate faster in G2 *tert*$^{-/-}$ than WT larvae, suggesting that telomere shortening in aging individuals could promote tumor progression in a noncell autonomous manner.

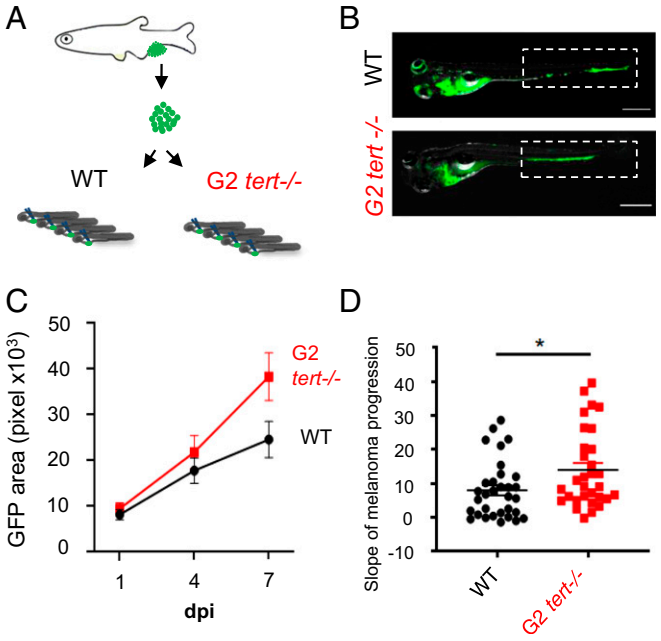

Fig. 3. G2 *tert*$^{-/-}$ larvae with very short telomeres exhibit increased melanoma expansion. (*A*) Experimental design for melanoma allotransplants in zebrafish larvae. Melanoma tumors were dissected from Tg(*mitfa:HRAS*^{G12V}*;β-actin:GFP*) zebrafish and cells dissociated. HRAS melanoma cells were then injected into blood circulation of 2-dpf zebrafish larvae. Larvae were kept for 7-d-postinjection (7-dpi). (*B*) Representative images of HRAS melanoma cells spread (green) in WT or G2 *tert*$^{-/-}$ larvae at 7 dpi. (Scale bars: 0.5 mm.) (*C*) Time course of HRAS melanoma cells spread in a group of WT and G2 *tert*$^{-/-}$ larvae ($P < 0.01$ at 7 dpi; WT $n = 10$; G2 *tert*$^{-/-}$ $n = 11$). (*D*) Melanoma tumors are more disseminated in G2 *tert*$^{-/-}$ larvae (*$P < 0.05$; WT $n = 32$; G2 *tert*$^{-/-}$ $n = 31$). A linear regression of three time points (1, 4, and 7 dpi) was used to calculate the slope of melanoma expansion over time. Each dot represents one larvae allotransplant.

G2 *tert*$^{-/-}$ Cells Are Senescent and Inflammatory and Capable of Modulating Their Surrounding Environment. Telomere shortening is responsible for replicative cell senescence in human cultured cells (37). Accordingly, we expected that *tert*$^{-/-}$ zebrafish would present increased levels of senescence. Indeed, we observed that the skin of *tert*$^{-/-}$ chimeras presented higher senescence (p15/16 immunofluorescence) when compared to the WT chimeras (Fig. 4 *A* and *B*). In contrast, melanoma tumor masses themselves showed similar levels of p15/16 in both WT and *tert*$^{-/-}$ chimeras (*SI Appendix*, Fig. S2 *A* and *B*).

Senescent cells secrete a set of molecules, known as SASP, mainly composed of inflammatory factors (21, 22). Therefore, we asked if *tert*$^{-/-}$ zebrafish present signs of inflammation. We measured TNF-α in the skin by immunofluorescence, and *tert*$^{-/-}$ chimeras showed significant higher levels of this cytokine when compared to the WT controls (Fig. 4 *A* and *C*). As before, the melanoma cell mass did not show a significant difference in TNF-α between WT and *tert*$^{-/-}$ chimeras (*SI Appendix*, Fig. S2 *A* and *C*). Our results indicate that the skin, a key tissue in melanoma initiation and progression, is senescent in the *tert*$^{-/-}$ chimeras and with signs of inflammation. However, these results were not observed in the tumor itself, suggesting that once melanoma is established, the TME is strongly modified by the tumor cells, and the genetic makeup of the host becomes less relevant.

Using RT-qPCR to investigate gene expression, we quantified the levels of senescence in *tert*$^{-/-}$ 9-mo-old adult tissues. The senescence markers *cdkn2a/b* (p15/16) and *cdkn1a* (p21) and TNF-α levels were significantly higher in the intestine of G1 *tert*$^{-/-}$ adults than WT controls (Fig. 4 *D*–*F*), suggesting that senescence and inflammation are systemic features of the *tert*$^{-/-}$ zebrafish. We also evaluated senescence and inflammation by RT-qPCR in 4-dpf G2 *tert*$^{-/-}$ larvae, and we observed that G2 *tert*$^{-/-}$ larvae present, like the adult zebrafish, significantly higher levels of senescence (p15/16 and p21; Fig. 4 *D* and *E*) and inflammation (TNF-α; Fig. 4*F*) compared to WT controls. In addition, using the SA-β-Gal assay, we confirmed higher levels of senescence were primarily localized to the head, notochord, and heart of G2 *tert*$^{-/-}$ larvae (Fig. 5*A*). Together, our results suggest that telomere shortening in zebrafish results in a systemic increase in senescence and inflammation.

Given the nature of these responses, we wanted to confirm if these observations originated from staining of *tert*$^{-/-}$ cells dispersed through the WT larvae or if *tert*$^{-/-}$ cells could modulate their extracellular environment in vivo and generate a systemic response. To test if short telomere *tert*$^{-/-}$ cells modulate their extracellular environment, we transplanted GFP-labeled G2 *tert*$^{-/-}$ cells during early development into WT recipient embryos thereby generating larvae chimeras (Fig. 5 *A* and *B*). Even though we transferred a few G2 *tert*$^{-/-}$ cells into developing embryos (<1% measured by fluorescence-activated cell sorting of desegregated embryos at 4 dpf), they were sufficient to increase overall SA-β-Gal levels (Fig. 5 *A* and *B*). Interestingly, we observed a similar pattern of SA-β-Gal staining in these chimeras as in G2 *tert*$^{-/-}$ larvae ($n = 22$) at the same stage of 4 dpf (compare Fig. 5 *A*, *Left* with Fig. 5*B*). These results suggest that cells derived from G2 *tert*$^{-/-}$ embryos are capable of inducing senescence in a noncell autonomous manner, thus, constituting an in vivo example of paracrine SASP.

Since senescent cells secrete proinflammatory molecules, we asked if G2 *tert*$^{-/-}$ cells with short telomeres could create an inflammatory environment in newly generated chimeras. To test

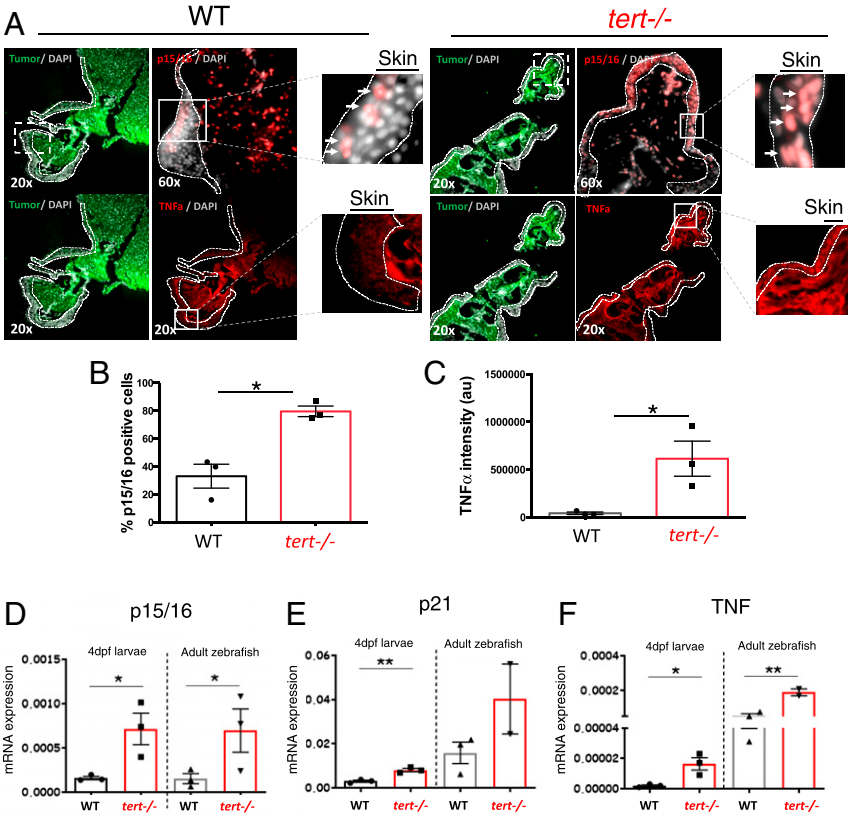

Fig. 4. *tert* $^{-/-}$ tissues present increased levels of senescence (p15/16) and inflammation (TNF-α). (*A*) Representative immunofluorescence images of p15/16 and TNF-α in the skin near melanoma in chimeric WT and *tert*$^{-/-}$ zebrafish. Dashed lines locate the skin (no green fluorescence), and arrows indicate p15/16-positive cells. Squares with dashed lines show place of amplification in a sequential section, and squares with solid lines show place of amplification on that section. (*B* and *C*) Quantification of p15/16-positive cells and levels of TNF-α, respectively, in the skin of chimeric WT and *tert*$^{-/-}$ zebrafish ($n = 3$). (*D–F*) RT-qPCR analysis comparing the expression levels of *cdkn2a/b* (p15/16), *cdkn1a* (p21), and *tnfa* (TNF) of 4-dpf WT, G2 *tert*$^{-/-}$ larvae, 9-months WT, and *tert*$^{-/-}$ adult intestine tissue. Data are represented as mean ± SEM. (*$P < 0.05$; **$P < 0.01$ for $n = 30$).

this, we generated similar embryo chimeras in Tg(*mpx:GFP*) recipient zebrafish that carry GFP-labeled neutrophils (38). As before, we injected both WT and G2 *tert*$^{-/-}$ cells from embryos at the blastula stage into Tg(*mpx:GFP*) recipient embryos of the same stage and observed its effects in 4-dpf larvae (Fig. 5*C*). Whereas WT cells generated zebrafish larvae ($n = 33$) with similar numbers of neutrophils as uninjected embryos, Tg(*mpx:GFP*) chimeras carrying G2 *tert*$^{-/-}$ cells ($n = 25$) exhibited higher numbers of neutrophils (Fig. 5*D*, $P = 0.0075$). Thus, since these innate immune cells are highly responsive in an inflammatory state, G2 *tert*$^{-/-}$ cells give rise to a systemic inflammatory environment. Together with the increased senescent markers and TNF1-α expression, our results indicate that telomerase-deficient zebrafish undergo senescence and produce an inflammatory state. Moreover, we show that this effect is noncell autonomous with *tert*$^{-/-}$ cells impacting the surrounding tissues, creating a systemic senescent and inflammatory environment.

Chemical Inhibition of Inflammation Rescues Melanoma Dissemination in the *G2 tert*$^{-/-}$ Mutant Larvae. Inflammation can induce transformed cell growth (39). In zebrafish, PGE_2 produced by innate immune cells via the COX-2 pathway was shown to act as key growth factor at the earliest stages of tumor progression (23, 40, 41). We hypothesized that the inflammatory environment induced by *tert*$^{-/-}$ cells could underlie the enhanced melanoma expansion observed in *tert* mutant zebrafish. To test this hypothesis, we treated the previously generated zebrafish melanoma larvae allografts with non-steroid anti-inflammatory drugs: aspirin (COX-1 and 2 inhibitor), and Celecoxib (COX-2-specific inhibitor). As previously, we measured melanoma dissemination by quantifying the GFP area at consecutive time points upon melanoma cell injections (1, 4, and 7 dpi). Both WT and G2 *tert*$^{-/-}$ recipients were kept in embryo medium containing aspirin (30 μM) or Celecoxib (25 μM) for the duration of the experiment. We calculated a progression slope of tumor cells per transplanted zebrafish and compared treated vs. untreated larvae (Fig. 6 *A–D*). As previously shown, melanoma cells exhibit an increased dissemination when transplanted into G2 *tert*$^{-/-}$ ($n = 31$) than in WT larvae ($n = 32$) (Fig. 3*D*, $P = 0.0205$). However, upon aspirin treatment, tumor cells disseminate in G2 *tert*$^{-/-}$ larvae ($n = 29$) with a very similar progression to WT controls ($n = 26$) (Fig. 6 *C* and *D*, aspirin $P = 0.5787$). Along the same line, melanoma progression in G2 *tert*$^{-/-}$ larvae ($n = 13$) is also similar to WT controls ($n = 19$) upon COX-2 inhibition with Celecoxib treatment (Fig. 6 *C* and *D*, Celecoxib: $P = 0.3523$). Both aspirin ($n = 26$) and Celecoxib ($n = 19$) treatments had no significant effect in the growth of tumor cells in WT tissues ($n = 32$) ($P = 0.3009$ and $P = 0.3189$, respectively). Together, our result suggests that the inflammatory environment induced by *tert*$^{-/-}$ cells promotes melanoma expansion via the COX-2 pathway. We showed an increase in innate immune cells in larvae containing telomerase-deficient cells (Fig. 5*D*). Thus, in agreement with previous studies (16, 33, 34), we propose that neutrophils, by producing larger amounts of prostaglandins, may enhance melanoma incidence.

Discussion

Studies on how telomerase affects tumorigenesis have focused primarily on the cell-autonomous role of telomere shortening in cancer cells (16). Indeed, telomerase is reactivated in the majority of cancer cells promoting cancer development. Consistently, telomerase

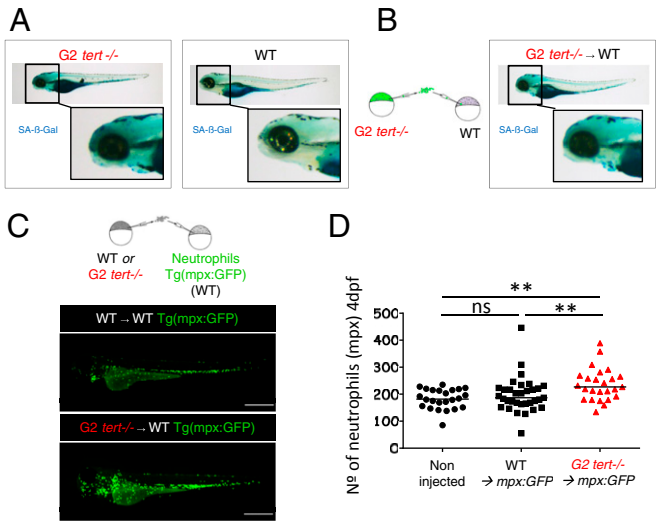

Fig. 5. G2 *tert* mutant cells induce high levels of senescence and systemic inflammation in host larvae. (*A*) Representative images of SA-β-Gal assay comparing WT and G2 $tert^{-/-}$ 4-dpf zebrafish embryos. Yolk sack staining is nonspecific. (*B*, *Left*) Scheme of chimera generation: G2 $tert^{-/-}$ blastula cells are transplanted into WT embryos (G2 $tert^{-/-}$ → WT). (*B*, *Right*) Marked senescence in 4-dpf WT embryos upon G2 $tert^{-/-}$ cell injection (*C*, *Left*) Scheme of chimera generation: WT or G2 $tert^{-/-}$ blastula cells transplanted into WT Tg(*mpx:GFP*) embryos with GFP-labeled neutrophils: WT → WT Tg(*mpx:GFP*) vs. G2 $tert^{-/-}$ → WT Tg(mpx:GFP). (*C*, *Right*) Representative images at 4 dpf, and neutrophils are shown in green. (Scale bars: 0.5 mm.) (*D*) Quantification of neutrophils at 4 dpf. Noninjected Tg(*mpx:GFP*) were used as controls. Each data point represents one zebrafish (**$P > 0.01$; noninjected $n = 24$; WT $n = 33$; $tert^{-/-}$ $n = 25$; ns, nonsignificant [$P > 0.05$]).

promoter mutations that result in increased telomerase expression are now recognized as one of the most common alterations in cancer (42). However, cancer incidence increases exponentially in the midages of human life, a time when telomeres are shorter (1, 2). In our current study, we attempted to understand why cancer incidence increases when telomeres are shorter. Apart from the recognized cell autonomous role in tumor suppression, we conclude that telomere shortening affects tumorigenesis in a noncell autonomous manner.

Seemingly, this hypothesis had been previously discarded: allotransplants of mouse melanoma cells gave rise to significantly smaller tumors in late generation (fifth generation [G5]) $Terc^{-/-}$ mice than in WT or G1 $Terc^{-/-}$ mice (10). This finding also correlated with impaired vascularization in the late generation telomerase-deficient mice. In contrast to our chimera experiments, the authors injected fully transformed melanoma cells, therefore, evaluating primarily tumor metastasis rather than tumor initiation and early progression. Late generation (G5) $Terc^{-/-}$ mice used in this study exhibit a severe phenotype and are likely to model very old human populations (85 y +) which have a significantly decreased risk of cancer. In our study, tumors arose typically at around 3 to 4 months of age when $tert^{-/-}$-associated phenotypes are initiating.

A study conducted by Ju and colleagues previously identified systemic effects caused by telomerase deficiency (43). Transplantation experiments showed that the function of WT hematopoietic stem cells was impaired in telomerase-deficient mice. Telomere dysfunction in the host mice increased systemic inflammatory signals, and this resulted, similar to aging animals, in a reduction in lymphopoieses while myelopoiesis was accelerated (43). Thus, as an organism grows older, increasing numbers of cells with short telomeres would modulate their surrounding environment creating a proinflammatory milieu potentially promoting tumorigenesis.

Using zebrafish embryo chimeras and cancer transplants, we show that incidence of melanoma is not only higher but progresses faster in animals deficient for telomerase. Both adult G1 $tert^{-/-}$ and G2 $tert^{-/-}$ embryos have shorter telomeres and mount DNA damage responses that stabilize p53 leading to premature aging and death (20, 32, 36). Indeed, mutations in *tp53* rescue the severity of both $tert^{-/-}$ models, allowing for prolonged survival. Spontaneous cancer in zebrafish, as in humans, is an age-associated disease that quickly rises upon decline of reproductive age (20, 44). Like other age-related phenotypes, spontaneous tumors in $tert^{-/-}$ zebrafish are accelerated to younger ages, while remaining similar in incidence and spectrum. Indeed, telomerase deficiency and telomere shortening in zebrafish do not appear to restrain tumorigenesis. Rather, they promote early cancer incidence denoting a systemic role in their effects. Similarly, humans with deficiencies in telomerase and premature telomere shortening show an increased cancer predisposition at younger ages (19). Thus, beyond preventing uncontrolled cell proliferation, the absence of telomerase and telomere shortening appears to have a systemic role impairing health status and resistance to disease.

How could telomere shortening in surrounding tissues lead to increased incidence of cancer? We observed that $tert^{-/-}$ zebrafish present high levels of senescence. Studies in vitro revealed that senescent cells secrete SASP, composed by several inflammatory factors (21, 22). In agreement, we observed that $tert^{-/-}$ zebrafish present high expression levels of *cdkn1a* and *cdkn2a/b* senescence genes and TNF-α, a cytokine involved in systemic inflammation. Moreover, G2 $tert^{-/-}$ cells are capable of inducing systemic senescence and inflammation in a noncell autonomous manner. These data constitute a strong indication that cells with

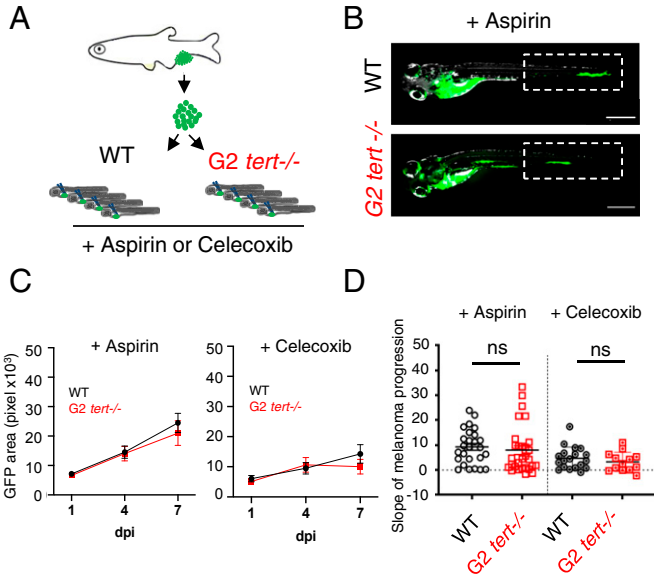

Fig. 6. Increased tumor expansion in G2 $tert^{-/-}$ larvae is rescued by inflammation inhibition. (*A*) Allotransplants of primary tumor cells extracted from melanoma in adult fish into 2-dpf larvae that were treated with aspirin or Celecoxib (COX-2 selective inhibitor). (*B*) Representative images of melanoma expansion at 7 dpi upon aspirin treatment. (Scale bars: 0.5 mm.) (*C*) Time course of melanoma dissemination in WT and G2 $tert^{-/-}$ larvae under aspirin treatment. (*D*) Slope of HRAS melanoma spread among 1, 4, and 7 dpi. Comparison of tumor cell expansion in a WT or G2 $tert^{-/-}$ treated with aspirin (WT $n = 26$ and G2 $tert^{-/-}$ $n = 29$) or Celecoxib (WT $n = 19$ and G2 $tert^{-/-}$ $n = 13$). Each dot represents one larva allotransplant. ns, nonsignificant ($P > 0.05$).

short telomeres are a source of paracrine SASP *in vivo.* However, similar to other studies in zebrafish (45), we were unable to detect other typical SASP cytokines in *tert*$^{-/-}$ zebrafish larvae, such as IL6 and IL10. The main in vivo SASP molecules are yet to be identified in zebrafish.

Consistent with higher levels of inflammatory cytokines, G2 *tert*$^{-/-}$ larvae containing critically short telomeres also exhibited an increased number of neutrophils. An increase in innate immune cells is characteristic of an inflammatory environment which can be tumorigenic. Human skin cancers have been shown to increase upon repeated injury and ulcers of previous lesions (46). In zebrafish, Feng et al. (23) showed that preventing the recruitment of innate immune cells reduced the growth of HRAS^{G12V}-transformed cells. Moreover, PGE2 produced by immune cells were shown to constitute a source of supportive signals for cancer cell growth. In line with this study, we observed a reduction of melanoma dissemination with anti-inflammatory treatment, such as aspirin and Celecoxib. Thus, our results suggest that a short telomere environment promotes the tumor development through the COX-2 pathway. It should be noted, however, that G2 *tert*$^{-/-}$ larvae represent models for both prematurely aged G1 *tert*$^{-/-}$ adults and naturally aged zebrafish. Just like tumor transplants in immunodeficient mouse models, the tumor microenvironment cannot be fully recapitulated in zebrafish larvae that lack, for example, a mature adaptive immune system.

Collectively, our data indicate that an environment with short telomeres promotes tumorigenesis in a noncell autonomous manner and increases proliferation and dissemination of melanoma cells. Apart from the recognized cell autonomous role in blocking uncontrolled cell division, telomere shortening, and senescence may have a second, perhaps, antagonistic pleiotropic consequence of causing local tissue damage and chronic inflammation. In fact, previous studies have shown that senescent fibroblasts induce proliferation of preneoplastic or neoplastic cells through paracrine factors (21, 47–49). SASP has also been shown to induce cancer migration and invasion by promoting epithelial-to-mesenchymal transition in tumor cells (50, 51). Thus, we propose that telomere shortening during aging gives rise to a systemic inflammatory environment. Chronic inflammation may be part of the mechanism whereby telomere shortening leads to increase tumorigenesis with age. Indeed, whereas chronic inflammation was shown to be a contributing factor in several cancers, immunosuppression leads to increase the risk for certain tumors (52, 53). Epidemiology studies associate the long-term dosage of aspirin with a reduced incidence of certain types of cancer (25–27). Interestingly, this effect is more pronounced with increased age of the population. Reverting telomere shortening in animal models that possess short telomeres, such as the zebrafish, will conclusively test the idea if repression of telomerase promotes cancer in aging.

Materials and Methods

Ethics Statement. All zebrafish work was conducted according to National Guidelines and approved by the Ethical Committee of the Instituto Gulbenkian de Ciência and the DGAV (Direcção Geral de Alimentação e Veterinária, Portuguese Veterinary Authority).

Zebrafish Maintenance and Standard Techniques. Zebrafish were maintained in accordance with Institutional and National animal care protocols. For normal line maintenance, embryos were collected from crosses and kept in E3 embryo medium (5.0-mM NaCl, 0.17-mM KCl, 0.33-mM CaCl, and 0.33-mM $MgSO_4$, 0.05% methylene blue, pH 7.4) at 28 °C on a 14-h light/10-h dark cycle. At 5 and 6 dpf, larvae were transferred into a recirculating system at 28 °C with a 14-h light/10-h dark cycle.

For anesthesia, fish were immersed into tricaine methane sulfonate solution at 168 μg/L (MS222 Sigma-Aldrich) and after the procedure placed back into system water. Their recovery was monitored until they regained normal swimming ability. Tricaine methane sulfonate was used at high concentration (200 mg/L) to euthanize fish. Larvae (until 7 dpf) were euthanized by placing them in ice-cold water for longer than 20 min.

Transgenic and Mutant Zebrafish Lines. The telomerase mutant line *tert*$^{AB/hu3430}$ generated by *N*-ethyl-nitrosourea mutagenesis (Utrecht University, Netherlands; Wienholds, 2004) has a *T→A* point mutation in the *tert* gene and is available at the ZFIN repository, ZFIN ID: ZDB-GENO-100412–50, from the Zebrafish International Resource Center. The *tert*^{hu3430} mutation was combined by genetic crossing in a *casper* background strain. *Casper* fish carry two germline mutations leading to the complete lack of pigmentation. The lack of melanocytes is caused by a mutation of the *mitfa* gene. In addition, the spontaneous *roy orbison* mutation causes the absence of iridophores and xantophores (54). For maintenance of this line, *casper; tert*$^{AB/hu3430}$ was continuously outcrossed to *casper; tert*$^{+/+}$. All recipient embryos used for the generation of HRAS chimeras, *tert*$^{-/-}$ homozygous mutants as well as their WT siblings were obtained by in crossing casper; *tert*$^{AB/hu3430}$ animals. Donor embryos carry two different transgenes: Tg(*mitfa:HRAS*^{G12V}*-mitfa:GFP;* β*-actin:membrane-bound GFP* [*mGFP*]). They express GFP and a mutated and oncogenic version of human HRAS under a melanocyte-specific promoter *mitfa* causing strong hyperpigmentation and the formation of melanoma (30). We used a Tg(β*-actin:mGFP*) line with ubiquitous expression of mGFP (55) since *mitfa:GFP* is only visible upon melanocyte development.

Generation of Zebrafish Chimeras. Both donor and recipient embryos were manually dechorionated using forceps (not earlier than 16 cell stage). Dechorionated embryos were maintained in transplant media (14.97-mM NaCl, 50- μM KCl, 1.29-mM CaCl2 · 2H2O, 150.63-μM KH_2PO_4, 50-μM Na_2HPO_4, and 994.04-μM $MgSO_4$ ·7H2O) with penicillin/streptomycin (100-U/mL penicillin and 100-μg/mL streptomycine) in agarose-coated plates until 48-h postfertilization after which they were transferred into E3 embryo medium in noncoated Petri dishes. Cell transfer from donor to recipient embryo was performed at the blastula stage using a hydraulic manual microinjector (CellTram vario, Eppendorf) with needles pulled from capillaries (TW100-4, World Precision Instruments with a tip clipped off and polished inner diameter at the tip 40–45 μm) using a fluorescent stereoscope (Leica M205FA). Labeled donor cells (GFP+) were taken from Tg(*mitfa:HRAS*^{G12V}*-mitfa:GFP;* β*-actin:mGFP*) embryos and injected into recipient embryos. Cells were taken up by gentle suction directly at the blastula surface and released by injecting into the blastula of the recipient without ever harming the yolk cell. To increase the likelihood of transferring neural crest progenitors for tumor studies in adult animals, cells were typically taken from three to five spots at different sides of the donor embryo, all aligned midway between animal pole and yolk cell. Directly upon transfer, around 5% (estimation) of cells in a chimeric embryo were donor derived. Single donor embryos served usually for various recipients (up to four), but one recipient never received cells from mixed donors. Upon cell transfer, embryos were kept at low density (maximum 50 per plate) at 28 °C and cleaned daily.

Selection of Chimeras to Grow and Tumor Assessment. All animals included in this study were screened for a normal phenotype, presence of melanocytes, and presence of GFP-positive donor cells. This screening was performed under light anesthesia (84-μg/L tricaine methane sulfonate MS222 in E3 embryo medium and 50% of standard concentration) under a fluorescence stereomicroscope (Leica M205FA).

Tumor appearance was assessed weekly and macroscopically. Individual animals were scored for the onset of a vertical growth phase, the presence of an outgrowth in any direction. Subsequently, most animals were analyzed by histopathology to confirm tumor formation and the state of invasiveness.

Fish Preservation for Histology. Fish were euthanized about 3 weeks upon the appearance of visible tumor masses or after reaching humane endpoints. When possible, fish were food deprived for 24 h prior to processing. After euthanizing, pictures of each fish were taken from both sides, both with a regular camera and at the fluorescent stereoscope (Leica M205FA) to save information about the gross distribution of pigmentation and chimeric (GFP+) cells. Animals were fixed in 10% neutral buffered formalin for 72 h at room temperature and decalcified in 0.5-M (ethylenedinitrilo)tetraacetic acid for 48 h. Whole fish were paraffin embedded, and 3-μm transversal cuts were performed from five to eight regions of the fish (depending on size). Cuts were stained with H and E and analyzed by histopathology. A total of $n = 18$ animals was analyzed (nine WT and nine *tert*$^{-/-}$ recipients).

Immunofluorescence and Microscope Analysis. Zebrafish sections were stained using a standard immunofluorescence protocol. Briefly, sections underwent deparaffinization by HistoChoice clearing agent (H2779, Sigma-Aldrich) for

20 min, followed by rehydratation, blocked (2% normal goat serum, 1% dimethyl sulfoxide [DMSO], and 0.01% Tween20 in 1× phosphate-buffered saline [PBS]) for 1 h at room temperature, followed by hybridization to primary antibody (1:50 PCNA [sc7907, Santa Cruz], 1:50 p16 [sc1661, Santa Cruz], 1:50 TNF-α [AS-55383, AnaSpec], and 1:100 GFP [632375, Clotech]) overnight at 4 °C. Samples were then incubated with a secondary antibody (1:500 anti-mouse-488 [A11001, Invitrogen] and 1:500 anti-rabbit-568 [A11036, Invitrogen]) overnight at 4 °C, followed by nuclear staining by DAPI (1:2,000). Fluorescence images were acquired by a DeltaVision microscope. Percentage of nuclear PCNA- or p15/16-positive cells was assessed in the whole skin or in the whole tumor section present in each image. TNF1-α levels were determined by assessing the integrated density of the signal by Fiji. For each quantification, a minimum of five fields per tumor ($n = 3$) were analyzed.

Melanoma Cell Transplants into 2-Dpf Larvae. Melanoma cells were derived from Tg(*mitfa:HRAS^{G12V}-mitfa:GFP*) zebrafish tumors. To obtain the tumor cells, fish were first euthanized with tricaine 25×, and the tumor was dissected with a regular scalpel and scissors. To dissociate the tumor, the mass of cells was dissected in small pieces, placed in a trypIE solution, and pipetted up and down. Enzymatic reaction was stopped with the addition of fetal bovine serum (FBS) (10% of the total volume). Solution was filtered (70-μm filter) and spun down at 1,700 rpm for 5 min. The pellet was resuspended in PBS calcium/magnesium free and then washed in culture medium with FBS (Dulbecco's modified Eagle's medium + 10% FBS). The final solution was ∼1 × 10^7 cells/mL and was obtained by removing as much supernatant as possible in the last centrifugation. One primary tumor was used per experiment ($n = 3$) from which 7–13 larvae were analyzed.

Melanoma cells were injected into the circulation of 2-dpf larvae with a microinjection apparatus, and needles were pulled from capillaries (TW100-4, World Precision Instruments). We injected 200–500 larvae, each with a calculated 50–100-nL cell suspension containing 1 × 10^7 cells/mL, providing a range of 500–1,000 melanoma cells per larva. Transplanted larvae were kept overnight at 28 °C in embryo media. On the following day, larvae were screened for the presence of GFP-positive cells in the tail region, and only those continued in the experiment. Pictures were taken at 1-, 4-, and 7-dpi using a fluorescent stereoscope (Leica M205FA). Transplanted larvae were kept in individual wells of a six-well plate to allow individual tracking of melanoma progression. GFP area measured in pixels was quantified using the Analyze Particles tool of imageJ 1.52i software. Upon linear regression of area values, we obtained an equation in the form of $y = a + bx$ in which the slope is provided by b, and it relates to the area differential over time.

Control (E3 medium) or treatment media (E3 medium containing aspirin—30 μM or Celecoxib—25 μM dissolved in DMSO) were replaced daily. The concentrations used for drug treatment are equivalent to LD50 dosages used in mice and humans for chronic treatments. Aspirin concentration was based on low-dose chronic treatment studies in humans with daily doses of typically around 2 mg/kg (27). LD50 of aspirin (determined in rodents) is ∼100× higher, we chose to equally treat our zebrafish daily with about 1% of LC50 which was published to be 567.7 mg/L in juveniles (56). Celecoxib, an inhibitor of prostaglandins E2 production, observed to prevent the expansion of HRAS transformed cells in the zebrafish larvae, was used at 25 μM according to Feng et al. (23), *SI Appendix, Supplemental Experimental Procedures*. These experiments were repeated two to three times.

Statistical Analysis. Statistical analysis was performed with the Software GraphPad Prism 6. Comparisons of two different points were performed by an unpaired t test. For the G1 HRAS chimeras, comparison over time (for, at least, two time points) was performed by two-way RM ANOVA. Histology analysis results depending on host genotype were compared using a χ^2 test. Tumor onset over time was compared using a log-rank (Mantel–Cox) test. A critical value for significance of $P < 0.05$ was used throughout the study. For the larvae transplants, trend lines of the GFP area among the three time points (1-, 4-, and 7-dpi) per transplanted zebrafish were calculated using Microsoft Excel 2010 software. Slope averages were compared between each two conditions using an unpaired t test with the Software GraphPad Prism 6.

Senescence-Associated β-Galactosidase Assay. β-galactosidase assay was performed as previously described (57). Briefly, euthanized zebrafish larvae were fixed overnight in 4% paraformaldehyde in PBS at 4 °C and then washed three times for 1 h in PBS-pH 7.4 and for a further 1 h in PBS-pH 6.0 at 4 °C. β-galactosidase staining was performed for 10 h at 37 °C in 5-mM potassium ferrocyanide, 5-mM potassium ferricyanide, 2-mM MgCl2, and 1-mg/mL X-gal in PBS adjusted to pH 6.0. After staining, larvae were washed three times for 5 min in PBS pH 7, observed, and photographed using a bright filter stereoscope (Leica M205FA).

Real-Time Quantitative PCR. Four-dpf larvae were euthanized, immediately snap frozen in liquid nitrogen, and collected in an Eppendorf tube, a minimum of 10 larvae each. RNA extraction was performed using a RNeasy extraction kit (Qiagen, UK no. 50974134). Briefly, larvae were smashed in RLT lysis buffer (provided by the kit), and the extract was washed and RNAs isolated through the RNA binding column and eluted in dH_2O RNase free, according to the manufacturer's procedures. Quality of RNA samples was assessed through BioAnalyzer (Agilent 2100, CA). Retrotranscription into complementary DNA (cDNA) was performed using a RT-PCR kit NZY First-Strand cDNA Synthesis Kit no. MB12501 (NZYtech). qPCR was performed using iTaq Universal SYBR Green Supermix no. 1725125 (Bio-Rad) and an ABI-QuantStudio 384 Sequence Detection System (Applied Biosystems, CA). qPCRs were carried out in triplicates for each cDNA sample. Relative mRNA expression was normalized to rpl13 mRNA expression using the discrete cosine transform method. Primer sequences are listed in *SI Appendix*, Table S1.

Data Availability. All data generated in this study are included in the paper and the *SI Appendix*.

ACKNOWLEDGMENTS. We thank members of the Telomeres and Genome Stability Laboratory for helpful discussions. We are grateful to Yi Feng (University of Edinburgh), Thiago Carvalho (Fundação Champalimaud), and Leonor Saúde (Instituto de Medicina Molecular) for critically reading our paper. We thank the Instituto Gulbenkian de Ciência Histology Unit and the IGC Fish Facility for excellent animal care. The IGC Fish Facility is financed by Congento LISBOA-01-0145-FEDER-022170, cofinanced by FCT (Portugal) and Lisboa2020 under the PORTUGAL2020 Agreement (European Regional Development Fund). K.L. was a recipient of a Portuguese FCT PhD fellowship SFRH/BD/52173/2013. B.L.-B. is a recipient of a French FRM postdoctoral fellowship (SPF201809007006). This work was supported by the FCT (Grants PTDC/BIM-ONC/3402/2014 and PTDC/SAU-ONC/116821/2010), Université Côte d'Azur - Académie 4 (Installation Grant: Action 2 - 2019) and the Howard Hughes Medical Institute International Early Career Scientist grant awarded to M.G.F.

1. D. M. Parkin, P. Pisani, J. Ferlay, Global cancer statistics. *CA Cancer J. Clin.* **49**, 33–64, 1 (1999).
2. G. Aubert, P. M. Lansdorp, Telomeres and aging. *Physiol. Rev.* **88**, 557–579 (2008).
3. W. Palm, T. de Lange, How shelterin protects mammalian telomeres. *Annu. Rev. Genet.* **42**, 301–334 (2008).
4. O. Samassekou, M. Gadji, R. Drouin, J. Yan, Sizing the ends: Normal length of human telomeres. *Ann. Anat.* **192**, 284–291 (2010).
5. X. Zhang, V. Mar, W. Zhou, L. Harrington, M. O. Robinson, Telomere shortening and apoptosis in telomerase-inhibited human tumor cells. *Genes Dev.* **13**, 2388–2399 (1999).
6. F. d'Adda di Fagagna *et al.*, A DNA damage checkpoint response in telomere-initiated senescence. *Nature* **426**, 194–198 (2003).
7. A. Lechel *et al.*, The cellular level of telomere dysfunction determines induction of senescence or apoptosis in vivo. *EMBO Rep.* **6**, 275–281 (2005).
8. K. L. Rudolph *et al.*, Longevity, stress response, and cancer in aging telomerase-deficient mice. *Cell* **96**, 701–712 (1999).
9. S. E. Artandi *et al.*, Telomere dysfunction promotes non-reciprocal translocations and epithelial cancers in mice. *Nature* **406**, 641–645 (2000).
10. S. Franco, I. Segura, H. H. Riese, Decreased B16F10 melanoma growth and impaired vascularization in telomerase- deficient mice with critically short telomeres. *Cancer Res.* **62**, 552–559 (2002).
11. E. González-Suárez, E. Samper, J. M. Flores, M. A. Blasco, Telomerase-deficient mice with short telomeres are resistant to skin tumorigenesis. *Nat. Genet.* **26**, 114–117 (2000).
12. Z. Ding *et al.*, Telomerase reactivation following telomere dysfunction yields murine prostate tumors with bone metastases. *Cell* **148**, 896–907 (2012).
13. Y. Begus-Nahrmann *et al.*, Transient telomere dysfunction induces chromosomal instability and promotes carcinogenesis. *J. Clin. Invest.* **122**, 2283–2288 (2012).
14. K. L. Rudolph, M. Millard, M. W. Bosenberg, R. A. DePinho, Telomere dysfunction and evolution of intestinal carcinoma in mice and humans. *Nat. Genet.* **28**, 155–159 (2001).
15. C. B. Harley, Telomerase and cancer therapeutics. *Nat. Rev. Cancer* **8**, 167–179 (2008).
16. J. W. Shay, W. E. Wright, Role of telomeres and telomerase in cancer. *Semin. Cancer Biol.* **21**, 349–353 (2011).
17. M. Armanios, E. H. Blackburn, The telomere syndromes. *Nat. Rev. Genet.* **13**, 693–704 (2012).
18. B. Holohan, W. E. Wright, J. W. Shay, Cell biology of disease: Telomeropathies: An emerging spectrum disorder. *J. Cell Biol.* **205**, 289–299 (2014).

19. B. P. Alter, N. Giri, S. A. Savage, P. S. Rosenberg, Cancer in dyskeratosis congenita. *Blood* **113**, 6549–6557 (2009).
20. M. C. Carneiro *et al*., Short telomeres in key tissues initiate local and systemic aging in zebrafish. *PLoS Genet.* **12**, e1005798 (2016).
21. J.-P. Coppé *et al*., Senescence-associated secretory phenotypes reveal cell-nonautonomous functions of oncogenic RAS and the p53 tumor suppressor. *PLoS Biol.* **6**, 2853–2868 (2008).
22. J.-P. Coppé, P.-Y. Desprez, A. Krtolica, J. Campisi, The senescence-associated secretory phenotype: The dark side of tumor suppression. *Annu. Rev. Pathol.* **5**, 99–118 (2010).
23. Y. Feng, S. Renshaw, P. Martin, Live imaging of tumor initiation in zebrafish larvae reveals a trophic role for leukocyte-derived PGE_2. *Curr. Biol.* **22**, 1253–1259 (2012).
24. Y. Feng, P. Martin, Imaging innate immune responses at tumour initiation: New insights from fish and flies. *Nat. Rev. Cancer* **15**, 556–562 (2015).
25. Y. Cao *et al*., Population-wide impact of long-term use of aspirin and the risk for cancer. *JAMA Oncol.* **2**, 762–769 (2016).
26. C. A. Gamba *et al*., Aspirin is associated with lower melanoma risk among postmenopausal Caucasian women: The Women's Health Initiative. *Cancer* **119**, 1562–1569 (2013).
27. P. M. Rothwell *et al*., Effect of daily aspirin on long-term risk of death due to cancer: Analysis of individual patient data from randomised trials. *Lancet* **377**, 31–41 (2011).
28. I. S. Kim *et al*., Microenvironment-derived factors driving metastatic plasticity in melanoma. *Nat. Commun.* **8**, 14343 (2017).
29. C. Tobia, G. Gariano, G. De Sena, M. Presta, Zebrafish embryo as a tool to study tumor/endothelial cell cross-talk. *Biochim. Biophys. Acta* **1832**, 1371–1377 (2013).
30. C. Michailidou *et al*., Dissecting the roles of Raf- and PI3K-signalling pathways in melanoma formation and progression in a zebrafish model. *Dis. Model. Mech.* **2**, 399–411 (2009).
31. E. E. Patton *et al*., BRAF mutations are sufficient to promote nevi formation and cooperate with p53 in the genesis of melanoma. *Curr. Biol.* **15**, 249–254 (2005).
32. C. M. Henriques, M. C. Carneiro, I. M. Tenente, A. Jacinto, M. G. Ferreira, Telomerase is required for zebrafish lifespan. *PLoS Genet.* **9**, e1003214 (2013).
33. A. I. Baba, C. Câtoi, "Tumor cell morphology" in *Comparative Oncology*, (The Publishing House of the Romanian Academy, 2007).
34. R. Fior *et al*., Single-cell functional and chemosensitive profiling of combinatorial colorectal therapy in zebrafish xenografts. *Proc. Natl. Acad. Sci. U.S.A.* **114**, E8234–E8243 (2017).
35. J. C. Moore, D. M. Langenau, "Allograft cancer cell transplantation in zebrafish" in *Advances in Experimental Medicine and Biology*, (Springer, 2016), pp. 265–287.
36. M. Anchelin *et al*., Premature aging in telomerase-deficient zebrafish. *Dis. Model. Mech.* **6**, 1101–1112 (2013).
37. R. C. Allsopp *et al*., Telomere length predicts replicative capacity of human fibroblasts. *Proc. Natl. Acad. Sci. U.S.A.* **89**, 10114–10118 (1992).
38. S. A. Renshaw *et al*., A transgenic zebrafish model of neutrophilic inflammation. *Blood* **108**, 3976–3978 (2006).
39. S. Ostrand-Rosenberg, Immune surveillance: A balance between protumor and antitumor immunity. *Curr. Opin. Genet. Dev.* **18**, 11–18 (2008).
40. C. A. Loynes *et al*., PGE_2 production at sites of tissue injury promotes an anti-inflammatory neutrophil phenotype and determines the outcome of inflammation resolution in vivo. *Sci. Adv.* **4**, r8320 (2018).
41. C. M. Freisinger, A. Huttenlocher, Live imaging and gene expression analysis in zebrafish identifies a link between neutrophils and epithelial to mesenchymal transition. *PLoS One* **9**, e112183 (2014).
42. B. Heidenreich, P. S. Rachakonda, K. Hemminki, R. Kumar, TERT promoter mutations in cancer development. *Curr. Opin. Genet. Dev.* **24**, 30–37 (2014).
43. Z. Ju *et al*., Telomere dysfunction induces environmental alterations limiting hematopoietic stem cell function and engraftment. *Nat. Med.* **13**, 742–747 (2007).
44. H. Feitsma, E. Cuppen, Zebrafish as a cancer model. *Mol. Cancer Res.* **6**, 685–694 (2008).
45. B. Novoa *et al*., Rag1 immunodeficiency-induced early aging and senescence in zebrafish are dependent on chronic inflammation and oxidative stress. *Aging Cell* **18**, e13020 (2019).
46. G. B. Maru, K. Gandhi, A. Ramchandani, G. Kumar, "The role of inflammation in skin cancer" in *Inflammation and Cancer*, B. Aggarwal, B. Sung, S. Gupta, Eds. (Springer, 2014).
47. A. Krtolica, S. Parrinello, S. Lockett, P. Y. Desprez, J. Campisi, Senescent fibroblasts promote epithelial cell growth and tumorigenesis: A link between cancer and aging. *Proc. Natl. Acad. Sci. U.S.A.* **98**, 12072–12077 (2001).
48. C. Bavik *et al*., The gene expression program of prostate fibroblast senescence modulates neoplastic epithelial cell proliferation through paracrine mechanisms. *Cancer Res.* **66**, 794–802 (2006).
49. K. Lawrenson *et al*., Senescent fibroblasts promote neoplastic transformation of partially transformed ovarian epithelial cells in a three-dimensional model of early stage ovarian cancer. *Neoplasia* **12**, 317–325 (2010).
50. I. Aifuwa *et al*., Senescent stromal cells induce cancer cell migration via inhibition of RhoA/ROCK/myosin-based cell contractility. *Oncotarget* **6**, 30516–30531 (2015).
51. V. Farsam *et al*., Senescent fibroblast-derived Chemerin promotes squamous cell carcinoma migration. *Oncotarget* **7**, 83554–83569 (2016).
52. L. Tang, K. Wang, Chronic inflammation in skin malignancies. *J. Mol. Signal.* **11**, 2 (2016).
53. S. Shalapour, M. Karin, Immunity, inflammation, and cancer: An eternal fight between good and evil. *J. Clin. Invest.* **125**, 3347–3355 (2015).
54. R. M. White *et al*., Transparent adult zebrafish as a tool for in vivo transplantation analysis. *Cell Stem Cell* **2**, 183–189 (2008).
55. M. S. Cooper *et al*., Visualizing morphogenesis in transgenic zebrafish embryos using BODIPY TR methyl ester dye as a vital counterstain for GFP. *Dev. Dyn.* **232**, 359–368 (2005).
56. E. Praskova *et al*., Acute toxicity of acetylsalicylic acid to juvenile and embryonic stages of Danio rerio. *Neuroendocrinol. Lett.* **33** (suppl. 3), 72–76 (2012).
57. S. Kishi *et al*., The identification of zebrafish mutants showing alterations in senescence-associated biomarkers. *PLoS Genet.* **4**, e1000152 (2008).